Mechanism of Heterogeneous Oxidation of Aluminum Powders

Keywords: Aluminum, Oxidation mechanism, Diffusion, Heterogeneous reaction

TA374

ABSTRACT

Thermal analysis is widely used to establish rates and mechanisms of oxidation of metal powders. For heterogeneous oxidation of aluminum, reaction may occur at the outer or inner surface of the growing oxide layer, depending on whether metal or oxidizer diffuse faster through that layer. A methodology of processing thermo-analytical measurements is introduced to distinguish such differences in the oxidation mechanism. The entire size distribution is considered for two spherical aluminum powders with different but overlapping particle sizes. The measured weight gain is distributed among particles of different sizes assuming that the rate of oxidation is proportional to the current reactive interface area. Three models are considered to determine the interface area. Weight gains for the same size particles from different powders were expected to be identical to each other when the model described the true oxidation mechanism. The results show that the reaction at the outer surface of a rigid oxide shell accurately describes the experiments. Thus, the outward diffusion of aluminum ions controls the rate of heterogeneous oxidation of aluminum in a wide range of temperatures from 400 – 1500°C.

INTRODUCTION

Aluminum oxidation leading to its ignition has been studied extensively [1-8]. The rate of oxidation is controlled by diffusion of oxygen and aluminum ions through a growing alumina scale. The diffusion rate experiences step-wise changes corresponding to polymorphic phase transitions occurring in the oxide [4, 5, 9, 10], and affecting its transport properties. It remains unclear which of the diffusing species, oxygen or aluminum diffuses faster – and where the reaction is occurring, inside or outside of the growing oxide layer. It has been proposed that aluminum diffuses faster through amorphous alumina [11], whereas diffusion of oxygen controls the reaction rate when crystalline alumina polymorphs are forming [11, 12]. Conversely, experiments and modeling efforts [2, 8, 13] suggest that outward diffusion of aluminum controls the reaction rate at a broad range of temperatures. Here, the reaction interface is identified based on processing previously published thermo-gravimetric (TG) experiments [9] on oxidation of two spherical aluminum powders with different but overlapping particle size distributions. Results are supported by Scanning Electron Microscopy (SEM) images of quenched samples.

TECHNICAL APPROACH

The reaction rate is assumed to be proportional to the available reactive surface while processing TG traces (Fig. 1) for two spherical Al powders by Alfa Aesar with nominal particle sizes of 3 – 4.5 and 10 – 14 μm. The particle size distributions for both powders (Fig. 2) are used to partition the mass increase inferred from the TG among powder particles in different size bins.

Three oxidation configurations were considered (Fig. 3). The initial oxide thickness was assumed to be 2.5 nm. The dimensions of aluminum core and alumina shell were assumed to change due to both oxidation and thermal expansion [14-17]. A change in aluminum density upon its melting was taken into account. For cases I and II, the oxide shell was assumed to be ductile: its dimensions were continuously minimized by the surface tension. For case I, the reaction was assumed to occur inside the growing alumina layer, at the aluminum/alumina interface. For case II, the reaction occurred at the outer layer of the ductile alumina shell. For case III, the oxide shell was treated as ductile before it reached its maximum radius; it became rigid and began separating from the aluminum core producing a void when the core radius started decreasing. In case III, similar to case II, the reaction was assumed to occur at the outer surface of the oxide shell.

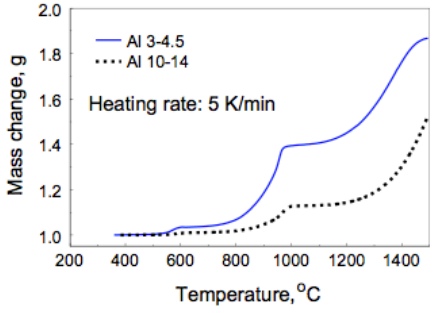

Figure 1: Oxidation weight gain for Al 3-4.5 and Al 10-14 from TG [9].

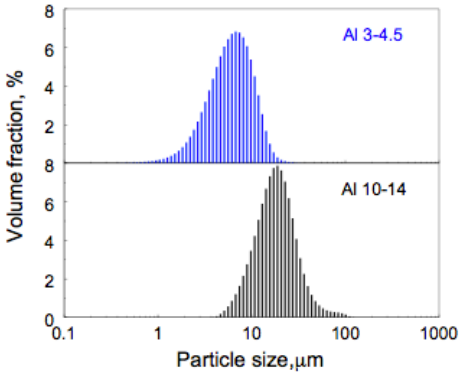

Figure 2: Particle size distribution for aluminum powders.

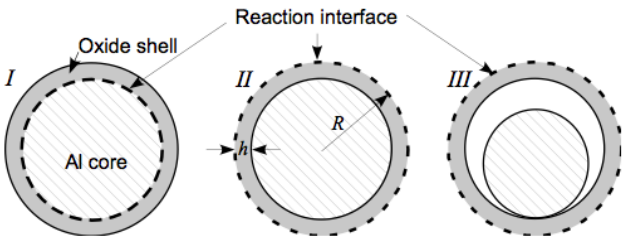

Figure 3: Schematic diagram of oxidation configurations considered: Case I: Ductile shell, reaction at the inner Al/Al_2O_3 interface; Case II: Ductile shell, reaction at the outer Al_2O_3 interface; Case III: Rigid shell, reaction at the outer Al_2O_3 interface.

ADDITIONAL EXPERIMENTS

TG experiments with both 3-4.5 µm and 10-14 µm powders were performed to recover and examine surface morphology of the partially oxidized particles. The experiments were conducted using a TA Instruments model Q5000IR thermogravimetric analyzer. The balance and the furnace were purged with argon at 10 ml/min and oxygen at 25 ml/min, respectively. The sample was heated at 5 K/min. A monolayer of aluminum particles was deposited on an alumina plate by coating it with a hexane-powder slurry. The plate was dried and placed in the TG sample pan. Samples were quenched at different temperatures. After quenching, the sample plate was carbon-coated and used in the SEM directly, without disturbing the powder.

RESULTS

Oxidation Of The Same Size Particles

Processing data in Fig. 1, oxidation dynamics for particles of identical sizes present in both powders were compared, as illustrated in Fig. 4. In each plot, the mass increase for particles in the size bin is calculated assuming cases I, II, and III (Fig. 3). It is apparent that the experimental data interpreted, assuming that the reaction occurs at the outer surface of the oxide, show a better match between the obtained mass change traces for identical particles belonging to different powders. Apparently, the best match for a 14.26-µm particle is found for case III.

Qualitative comparisons, illustrated in Fig. 4, were supplemented by a quantitative comparison of calculated oxidation traces for all overlapping particle size bins. Differences between the mass change traces for each size bin were assessed calculating a square root of the square error:

$$Er = \sqrt{\frac{\sum_j \left(\Delta m_{j1} - \Delta m_{j2}\right)^2}{J}} \qquad (1)$$

where Δm_{j1} is the percent weight change for sample Al 3-4.5; Δm_{j2} is the percent weight change for sample Al 10-14, both taken for the j-th time step; and J is the total number of time steps in the experiment.

The calculated results for three cases are plotted in Fig. 5. The model with the smallest value of Er is expected to better describe the oxidation event. It is apparent that both cases II and III are better than case I.

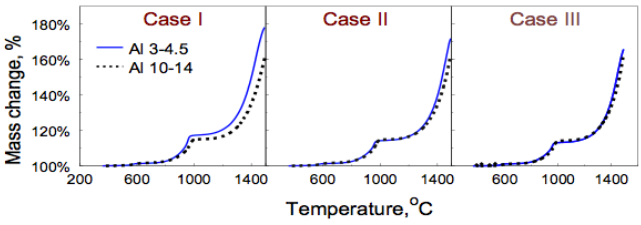

Figure 4: Calculated mass increase for a 14.26 µm diameter Al particle as a function of temperature.

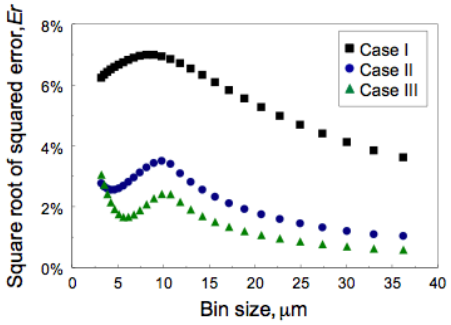

Figure 5: The squares of difference between the weight gain curves calculated for two samples for different size bins (see Eq. 1).

Surface morphology

Figure 6 shows particles quenched at different temperatures. At 750°C, surfaces exhibit concave depressions, likely formed due to the shrinkage of the thermally expanded particles upon quenching. At higher temperatures, depressions on particle surfaces no longer exist. Instead, particles retain roughly spherical shapes. At 850°C, surface oxide grain boundaries become noticeable. At 950°C, crystallites are observed to grow at the grain boundaries. The crystallites become prominent at 1050°C. Qualitatively, similar images are also observed for undisturbed aluminum 10-14 µm. The features are less prominent for 10-14 µm due to a lesser degree of reaction completion.

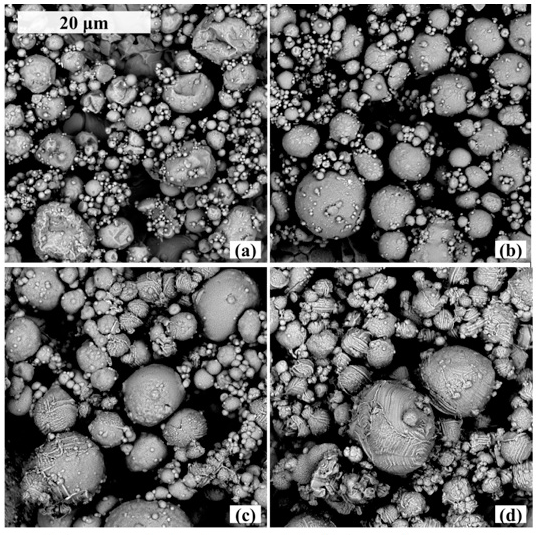

Figure 6: Images of aluminum particle (3-4.5 µm) quenched at 750 (a), 850 (b), 950 (c) and 1050°C (d). Note: sample surface is intact after oxidation and quenching.

In addition to the undisturbed particles previously discussed, particles broken into several pieces as a result of handling were examined (Fig. 7). It appears that aluminum particles oxidize forming a hollow oxide shell partially filled with molten aluminum.

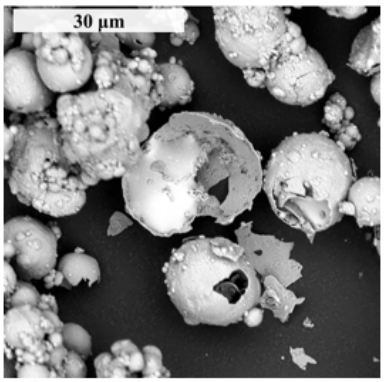

Figure 7: Images of aluminum particle (10-14 µm) quenched at 950°C. Sample surface is disturbed.

DISCUSSION

Based on the comparison of different reaction scenarios, in particular from Figs.4 and 5, it is concluded that the reaction occurs at the outer surface of the growing oxide, and thus the outward diffusion of aluminum ions is faster than the inward diffusion of oxygen ions during oxidation of aluminum powders. Case III describes oxidation better for all except for the two smallest particle size bins considered, offering the best approximation to the actual oxidation scenario. It is assumed that the oxide shell becomes rigid when the particle reaches its maximum radius. The discrepancy for small particles can be explained by the fact that small particles reach their maximum radius at the very beginning, and thus are treated as rigid particles throughout the calculation. It was recently reported [18], that aluminum oxide shells become rigid when their thickness reaches about 20 nm. This calculation shows that larger size oxide shells would grow to a greater thickness, approximately 100 nm, before they become rigid. It appears that for a larger particle, the maximum size of the aluminum core is reached when it expands due to melting, after which it remains nearly constant until about 850°C, when the shrinkage due to consumption of aluminum exceeds the effect of thermal expansion. If a particle is quenched from 750°C, it will solidify so that the Al core will shrink noticeably. An expanded ductile oxide shell may collapse, forming depressions (Fig. 6). The oxide thickness expected to form at these temperatures is just under 100 nm, indicating that this is likely the thickness at which the oxide became rigid. At higher temperatures, the shell thickness increases and it becomes rigid. When the aluminum core shrinks further during its consumption or even upon quenching and solidification, the oxide shell preserves its spherical shape, cf. Fig. 6, 7. The shells in Fig. 7 contain what appears to be a pool of aluminum, however they remain spherical. The thickness of the observed broken shells is close to 100 nm.

The crystallites observed to grow at the alumina grain boundaries at high temperatures (Fig. 6) are likely to indicate that once the oxide layer becomes crystalline, the GRAIN boundary diffusion is much faster than its inter-crystalline counterpart. The well-preserved structures of the externally growing crystallites support the conclusion that their growth is controlled by the outward diffusion of aluminum.

CONCLUSION

A data processing method is established to identify the location of heterogeneous reaction controlled by diffusion of reacting species through a growing product layer. The method is applied to study oxidation of aluminum powders by processing respective TG measurements. The experimental data are well interpreted assuming that the reaction occurs at the outer surface of the growing rigid oxide layer and thus is controlled by the outward diffusion of aluminum ions. The growing oxide shell becomes rigid once its thickness reaches approximately 100 nm. Oxide shells reaching this thickness do not shrink together with the consumed aluminum core, so hollow particles are formed as a result of oxidation.

ACKNOWLEDGEMENT

This work was submitted by Shasha Zhang and Edward L. Dreizin as part of the Student Award Program. This work was supported by the Defense Threat Reduction Agency.

REFERENCES

1. M.M. Mench, K.K. Kuo, C.L. Yeh, Y.C. Lu, Combustion Science and Technology, 135 (1998) 269-292.

2. A. Rai, K. Park, L. Zhou, M.R. Zachariah, Combustion Theory and Modelling, 10 (2006) 843-859.

3. M.A. Trunov, M. Schoenitz, E.L. Dreizin, Propellants, Explosives, Pyrotechnics, 30 (2005) 36-43.

4. M.A. Trunov, M. Schoenitz, X. Zhu, E.L. Dreizin, Combustion and Flame, 140 (2005) 310-318.

5. M.A. Trunov, S.M. Umbrajkar, M. Schoenitz, J.T. Mang, E.L. Dreizin, Journal of Physical Chemistry B, 110 (2006) 13094-13099.

6. K.W. Watson, M.L. Pantoya, V.I. Levitas, Combustion and Flame, 155 (2008) 619-634.

7. M. Schoenitz, B. Patel, O. Agboh, E.L. Dreizin, Thermochimica Acta, 507-508 (2010) 115-122.

8. B.J. Henz, T. Hawa, M.R. Zachariah, Journal of Applied Physics, 107 (2010), 024901.

9. M.A. Trunov, M. Schoenitz, E.L. Dreizin, Combustion Theory and Modelling, 10 (2006) 603-623.

10. M. Schoenitz, B. Patel, O. Agboh, E.L. Dreizin, Thermochimica Acta, 507-508 (2010) 115-122.

11 L.P.H. Jeurgens, W.G. Sloof, F.D. Tichelaar, E.J. Mittemeijer, Journal of Applied Physics, 92 (2002) 1649.

12. L.P.H. Jeurgens, W.G. Sloof, F.D. Tichelaar, E.J. Mittemeijer, Thin Solid Films, 418 (2002) 89-101.

13. B.J. Henz, T. Hawa, M.R. Zachariah, Molecular Simulation, 35 (2009) 804-81.

14. A.J.C. Wilson, Proceedings of the Physical Society, (1941) 9.

15. W.D. Drotning, Master Dissertation, Sandia Laboratories, 1979.

16. O. Sarikaya, Materials & Design, 26 (2005) 53-57.

17. M. Munro, Journal of the American Ceramic Society, 80 (1997) 1919-1928.

18. B. Rufino, M.V. Coulet, R. Bouchet, O. Isnard, R. Denoyel, Acta Materialia, 58 (2010) 4224-4232.

For more information or to place an order, go to http://www.tainstruments.com/ to locate your local sales office information.